MASSACHUSETTS INSTITUTE OF TECHNOLOGY
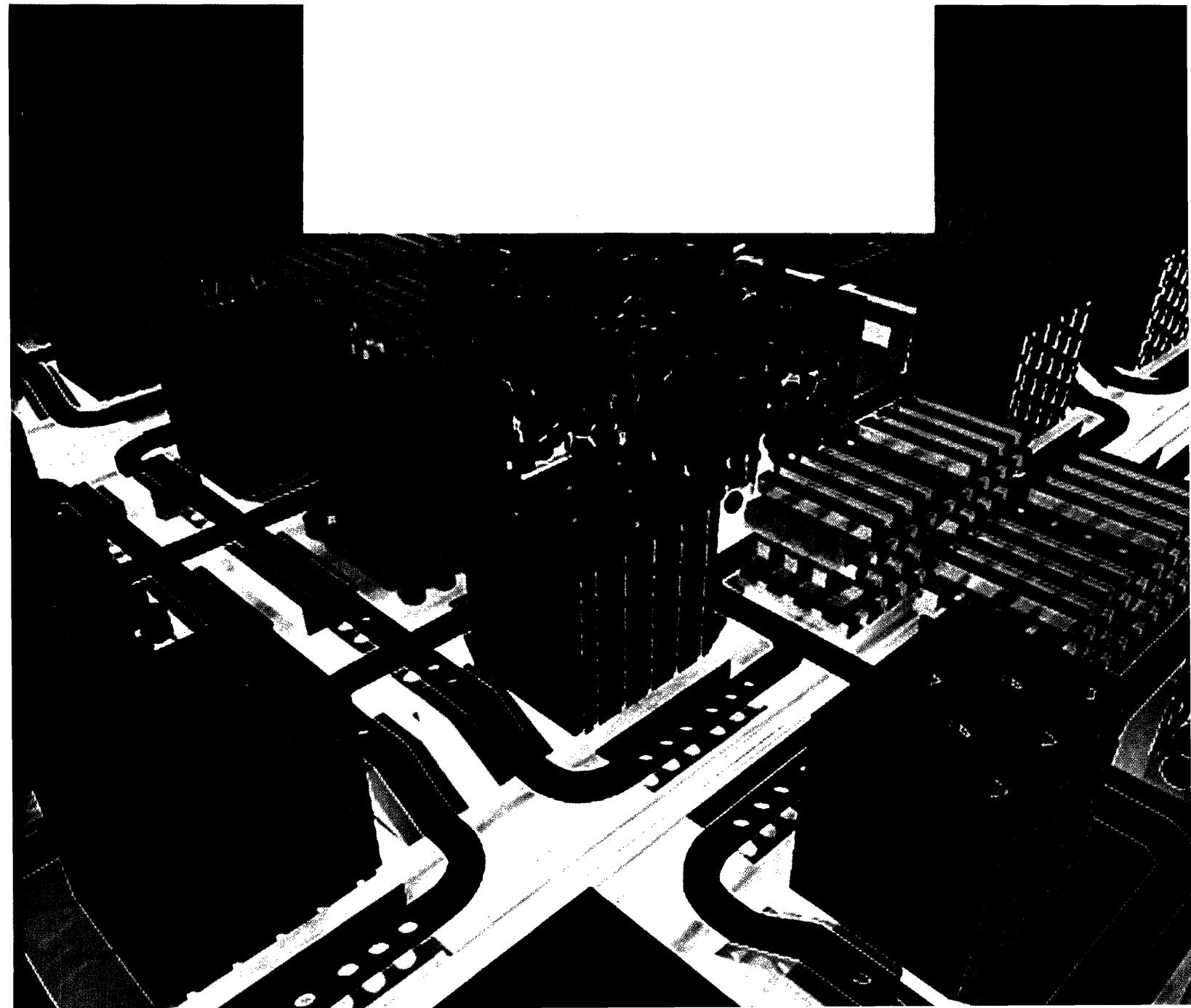## *The* RESEARCH LABORATORY *of* ELECTRONICS
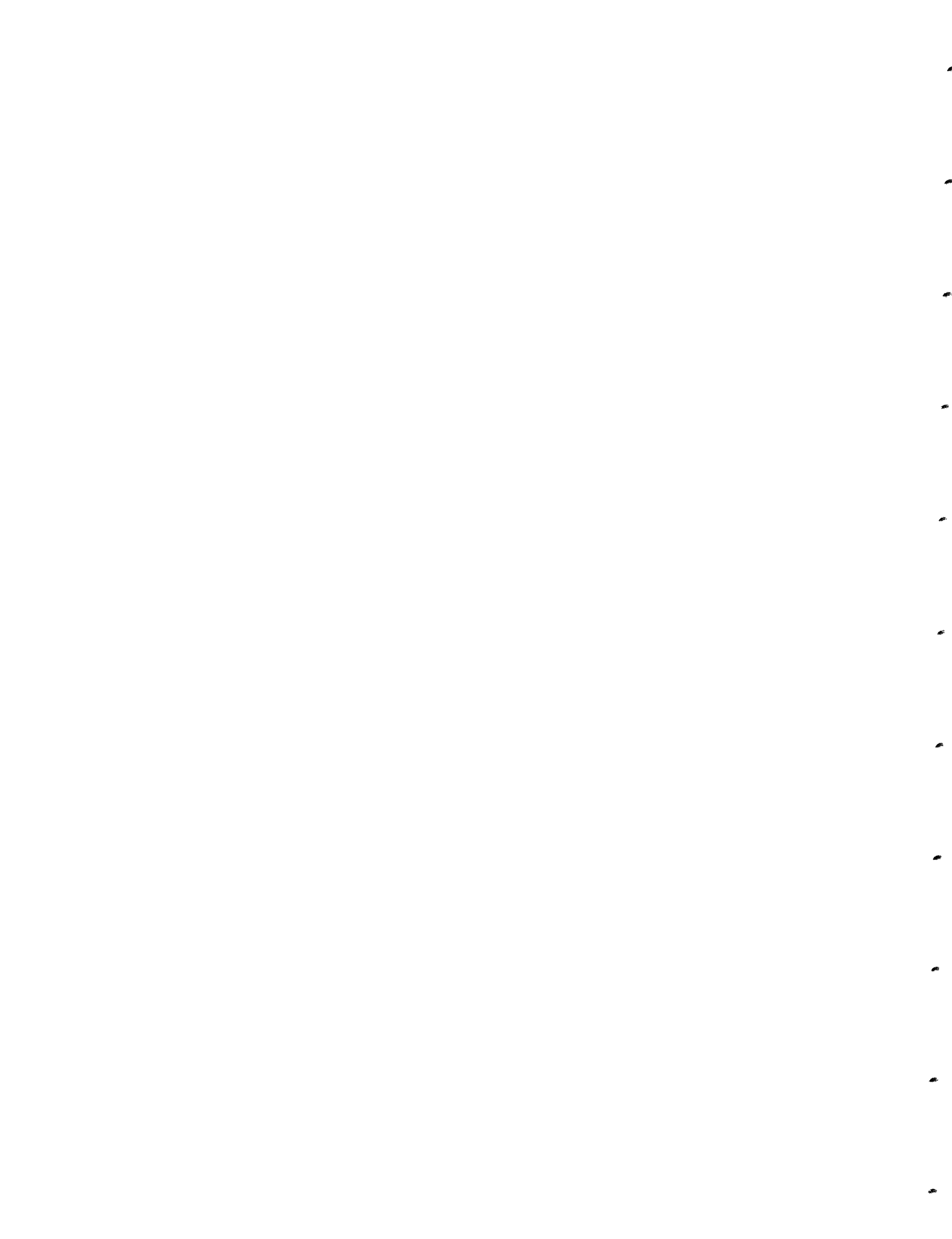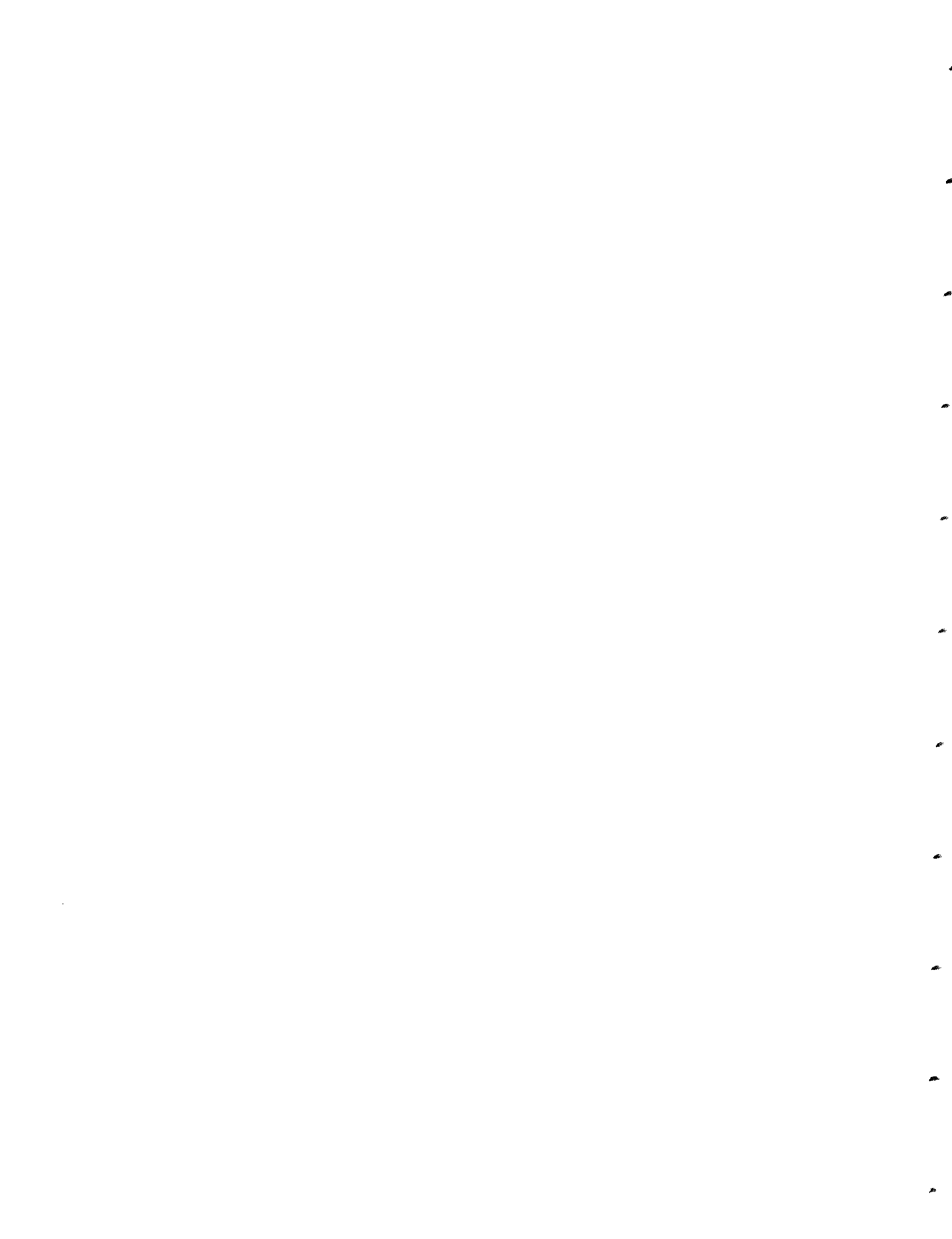
Vortices and Interferences in Bose-
Einstein Condensates

By: Till Rosenband

RLE Technical Report No. 655

June 2001

Vortices and Interferences in Bose-Einstein Condensates

By: Till Rosenband

RLE Technical Report No. 655

June 2001

Vortices and Interference in Bose-Einstein Condensates

by

Till Rosenband

Submitted to the Department of Physics
in partial fulfillment of the requirements for the degree of

Bachelor of Science

at the

MASSACHUSETTS INSTITUTE OF TECHNOLOGY

June 2001

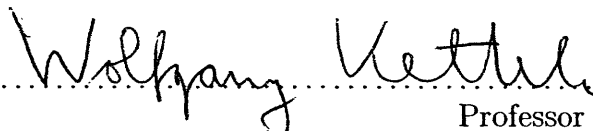© Till Rosenband, 2001. All rights reserved.

Author . . . .
Department of Physics
May 23, 2001

Certified by . . . .
Professor Wolfgang Ketterle
Thesis Supervisor, Department of Physics

Accepted by . . . .
Professor David E. Pritchard
Senior Thesis Coordinator, Department of Physics

Vortices and Interference in Bose-Einstein Condensates
by
Till Rosenband

Submitted to the Department of Physics
on May 23, 2001, in partial fulfillment of the
requirements for the degree of
Bachelor of Science

Abstract

This thesis is the result of my participation in a study of vortices and interference in BEC. Vortices were created by stirring a laser beam through a Bose condensate, and observing the resulting phase singularities in interference images. Computer software and electronics were contributed to this study. Improvements to the experiment's imaging system were devised that eliminate most of the non-statistical background noise in our images. An alternative optical path to the regular probe beam path was constructed that electronically deflects the probe beam and illuminates the condensate from various angles in order to smooth out the effects of unwanted interference in the beam. Electronic circuitry was designed and built that rapidly and reproducibly sweeps the probe beam through the imaging system.

Thesis Supervisor: Professor Wolfgang Ketterle
Title: Thesis Supervisor, Department of Physics

Acknowledgments

This thesis would not have been completed without the support of many generous individuals. People who were extremely busy with their own work found the time to help me along with my endeavors.

My deepest gratitude goes to Professor Ketterle who is not only one of the finest researchers and teachers, but also the best advisor I could have had. Without his encouragement I would have thrown in the towel long ago. Axel Görlitz has provided invaluable advice, both in the lab and at the editing desk. He taught me how to "walk" a laser beam and align an optical fiber. I have learned a great deal of physics from Shin "Anyway" Inouye. His wonderful gift for intuitive explanations will be of great advantage to future students. Deep Gupta taught me about AOMs and was an irreplaceable partner in my quest to improve our imaging system. His ideas were seminal to the entire project.

During my years at MIT I spent many enjoyable days and nights among the Ketterle BEC group. The lab and its members were often a source of brightness among otherwise dreary days at the Institute. Jamil Rashid Abo-Shaeer needs to be mentioned for his constant good cheer and aura of "Green Mountain Time". Aaron, Todd, Zoran, Johnny, Robert, Martin, Claudiu, Ananth, Kai, and Chandra all helped me out in big ways and small. They were not only colleagues, but good friends.

I owe the greatest debt to my family who supported me throughout my studies at MIT and adopted my many problems as their own. That debt can never be repaid.

In addition I would like to acknowledge the Studienstiftung des deutschen Volkes for their generous and unquestioning support.

Contents

List of Figures

Chapter 1

Introduction and Overview

Bose-Einstein Condensation (BEC) is a peculiar state of matter whose existence is due solely to the indistinguishable nature of particles. This state was first proposed by S. N. Bose and Albert Einstein in 1924-25. During the 75 years after their initial proposal theoretical discussion of BEC progressed, but experimental investigation of the area was hindered by the fact that until 1995 BEC could only be created in strongly interacting systems like ^{4}He and superconductors. The textbook example of BEC is a non-interacting gas of Bosons [1]. In 1995 experimentalists finally succeeded in condensing a weakly interacting gas [2, 3, 4]. This new gaseous BEC, while hard to produce, is well described theoretically, and easily probed and manipulated using lasers and magnetic fields. During the past 5 years experimenters have busily explored some of the exciting features of BEC that were predicted many years ago but until recently were not accessible to laboratory study.

One of the most dramatic results in BEC research was the observation of the interference of matter waves [5]. When two BECs were placed side-by-side and allowed to expand, they produced interference fringes analogous to the interference of coherent light emitted by two point sources. Contrary to the most basic everyday experience about how matter behaves, when two gases were combined their densities did not add up like densities at all. Rather the densities added in some places and subtracted in others. This experiment showed that a Bose condensate is a single giant quantum mechanical matter wave described by a single phase and that two BECs can interfere just like any two ordinary waves.

Closely related to quantum phase in BEC, and of great theoretical interest, are vor-

tices. In a BEC without angular momentum the phase is continuous single-valued function throughout the sample. Vortices radically change the quantum phase by causing it to increase by an integer multiple of 2π along any closed path around the vortex. This altered phase geometry should be clearly visible when a BEC containing a vortex interferes with an undisturbed condensate.

This thesis describes the experimental effort to observe vortices by splitting a condensate in half, stirring one half with a laser beam, and then causing it to interfere with the other half. Chapter 2 gives a brief introduction to BEC. A brief outline of our apparatus appears in Chapter 3. Vortices and interference between BECs are described in Chapter 4. Chapter 5 documents a technique I developed that improves the image quality in our apparatus. This technique was used in our efforts to observe vortices. A paper submitted for publication that describes our vortex study is included as Appendix A.

Chapter 2

What is BEC?

Bose condensation is a phase transition that occurs at very low temperatures. It leads to a strange state of matter whose existence is due entirely to the quantum statistics of bosons. Below the condensation temperature most bosons occupy the quantum mechanical ground state of the system they inhabit. This macroscopic occupation of the ground state leads to amazing phenomena such as superconductivity and superfluidity. The first part of this chapter explains how quantum statistics leads to Bose condensation in a non-interacting bosonic gas, while the second part describes an equation that gives insight into the dynamics of a weakly interacting BEC.

2.1   Quantum Statistics of Bosons and Fermions

Any description of the world must reflect the fact that identical particles are indistinguishable at the most basic level [6]. If two electrons are exchanged, reality is unaffected, and all physical equations must conform to this principle. Equations that describe a world indifferent to particle exchange are referred to as symmetrized. The equations of classical physics are automatically invariant under particle exchange. In wave mechanics the most basic reality is the wave function which is not an observable. Since all observables are unaffected by the sign of the wave function, the wave function is allowed to change sign under particle

exchange. Therefore, for two identical particles in states ψ_a and ψ_b one can write

$$\psi_+(\mathbf{r_1}, \mathbf{r_2}) = [\psi_a(\mathbf{r_1})\psi_b(\mathbf{r_2}) + \psi_b(\mathbf{r_1})\psi_a(\mathbf{r_2})]/\sqrt{2} \tag{2.1}$$

$$\psi_-(\mathbf{r_1}, \mathbf{r_2}) = [\psi_a(\mathbf{r_1})\psi_b(\mathbf{r_2}) - \psi_b(\mathbf{r_1})\psi_a(\mathbf{r_2})]/\sqrt{2} \tag{2.2}$$

Where

$$\psi_+(\mathbf{r_1}, \mathbf{r_2}) = \psi_+(\mathbf{r_2}, \mathbf{r_1}) \tag{2.3}$$

$$\psi_-(\mathbf{r_1}, \mathbf{r_2}) = -\psi_-(\mathbf{r_2}, \mathbf{r_1}). \tag{2.4}$$

Equation 2.3 holds for all particles of integer spin (bosons), while Equation 2.4 is true for all particles whose spin is an odd multiple of 1/2 (fermions). Equation 2.2 shows that it is impossible for two fermions to ever occupy the same quantum state, for if $\psi_a = \psi_b$ then $\psi_- = 0$, which can not be normalized. However, Equation 2.1 shows that bosons can readily occupy the same quantum state and this fact, along with the knowledge that identical particles are indistinguishable, will be central ideas for the following discussion.

2.2   Bose Condensation

Bose condensation is defined as the condition in which a macroscopic fraction of a system's particles inhabits the ground state [7]. While it is not surprising that most of the particles in a system can be frozen into the ground state if enough energy is removed, it is remarkable that BEC occurs at temperatures where the thermal energy $k_B T$ is much larger than the energy level spacing $\hbar\omega$. To see why this is possible it is useful to recall the definition of temperature [8]

$$\frac{1}{k_B T} = \frac{\partial S}{\partial E}. \tag{2.5}$$

This can be rewritten by approximating the derivative with finite differences, and substituting $S = \log \Omega$ where Ω is the number of accessible states:

$$\frac{1}{k_B T} \approx \frac{S_2 - S_1}{E_2 - E_1} = \frac{\log \Omega_2/\Omega_1}{E_2 - E_1}. \tag{2.6}$$

12

For the sake of simplicity we shall assume a system of 1-D harmonic oscillators[1] whose energy is quantized in units of $\hbar\omega$. We then arrive at the result

$$k_B T(E, N) \approx \frac{\hbar\omega}{\log\left[\Omega(E + \hbar\omega, N)/\Omega(E, N)\right]}. \tag{2.7}$$

In order to evaluate 2.7 we must find the value of $\Omega(E, N)$. Assuming a macroscopic population of the ground state, Ω is a function only of E, which equals the number of combinations of positive integers that add up to $n = E/\hbar\omega$. This is also known as the number of partitions of n, which has been famously approximated by Ramanujan as [10]

$$\Omega(n\hbar\omega) = \frac{e^{\pi\sqrt{2n/3}}}{4n\sqrt{3}}. \tag{2.8}$$

When this approximation is substituted into 2.7 it follows that

$$
\begin{aligned}
k_B T(n\hbar\omega) &\approx \frac{\hbar\omega}{\log\frac{n}{n+1} + \pi\sqrt{\frac{2}{3}}(\sqrt{n+1} - \sqrt{n})} \\
&= \frac{\hbar\omega}{-\log\left(1 + 1/n\right) + \pi\sqrt{\frac{2n}{3}}(\sqrt{1 + 1/n} - 1)} \\
&\approx \frac{\hbar\omega}{-1/n + \frac{\pi}{\sqrt{6n}}} \\
&\approx \frac{\sqrt{6n}}{\pi}\hbar\omega.
\end{aligned}
\tag{2.9}
$$

This calculation shows that a system of N particles with average energy $\bar{\epsilon} = \hbar\omega$ has a temperature which is greater by a factor of $\frac{\sqrt{6N}}{\pi}$ than the single particle case.

Equation 2.9 is a lower limit for the condensation temperature of n particles in a 1-D harmonic oscillator potential. At this energy atoms are just beginning to freeze into the ground state, and the chemical potential is 0, since any atoms added to the system while holding the total energy constant *must* occupy the ground state. The exact transition

---

[1]Although it has been suggested that BEC in 1-D harmonic systems is not possible, BEC does occur in finite 1-D harmonic systems [9].

13

temperature for a 1-D BEC [9] is given by

$$n = \frac{k_B T_c}{\hbar \omega} \log\left(\frac{2 k_B T_c}{\hbar \omega}\right). \tag{2.10}$$

For large n we can approximate $\log\left(\frac{2 k_B T_c}{\hbar \omega}\right)$ by $\log(2n)$. This gives the result

$$k_B T_c = \frac{n}{\log(2n)} \hbar \omega, \tag{2.11}$$

which exceeds the lower bound given in Equation 2.9.

2.3 Transition Temperature

While the arguments in Section 2.2 make a case for the existence BEC, they provide little insight into the critical temperature T_c at which 3-D condensation occurs. Dimensional analysis provides the easiest approach to calculating T_c [11]. The only macroscopic parameter describing the system that is independent of size and temperature is the number density n. The physical constants that factor into the calculation are $\hbar$, k_B, and the mass of each particle m. The units associated with these four values can be combined in only one way to yield a temperature:

$$T_c \propto \frac{\hbar^2 n^{2/3}}{m k_B} \tag{2.12}$$

A different argument leading to the same conclusion is that when the temperature is low enough so that the thermal deBroglie wavelength λ_{dB} approaches the interparticle spacing, condensation occurs due to wavefunction overlap. This condition is expressed by

$$n^{-1/3} = \lambda_{dB} = \sqrt{\frac{2\pi \hbar^2}{m k_B T_c}}$$
$$T_c = \frac{2\pi \hbar^2 n^{2/3}}{m k_B}, \tag{2.13}$$

which agrees with Equation 2.12. A more rigorous treatment using Bose-Einstein statistics [12] yields the correct proportionality constant for a non-interacting ideal gas in a rigid

enclosure of volume V,

$$T_c = \left[\frac{n}{\zeta(3/2)}\right]^{2/3} \frac{2\pi\hbar^2}{mk_B},$$ (2.14)

where $\zeta(3/2) \approx 2.6$ is the Riemann zeta function. In our BEC apparatus the atoms are trapped by magnetic fields which provide a harmonic trapping potential. In this case the transition temperature is [13]

$$T_c = \left[\frac{N\omega_x\omega_y\omega_z}{\zeta(3)}\right]^{1/3} \frac{\hbar}{k_B}.$$ (2.15)

A typical case from our lab is $N \approx 10^7$, $\omega_x = \omega_y = 2\pi \times 165\text{Hz}$, and $\omega_z = 2\pi \times 16\text{Hz}$. Using $\zeta(3) \approx 1.2$ we find $T_c \approx 740\text{nK}$.

2.4 Dynamics of BEC

The previous sections have provided a description of the static properties of BEC. However, our experimental work investigated the dynamic behavior of vortices in a BEC superfluid. To see how atoms move within the condensate we shall assume that all of the atoms occupy the ground state, and ignore the uncondensed atoms. All the atoms we seek to describe are in the ground state, but this state itself is modified by the presence of other atoms. Since our sodium BEC is a weakly interacting gas, rather than a non-interacting gas, we must account for the effects that the atoms have on one another.

A commonly used model reflects only the effects of two-body interactions. Neglecting many-body interactions is justified, since BEC is a dilute gas. This model can be understood intuitively by remembering that all Bose condensed atoms have the same single particle wave function. Therefore we need only one wave function to describe all of the atoms at once! This giant wave function is called the order parameter Φ, and its time evolution is given by the Gross-Pitaevskii (GP) equation [13]

$$i\hbar\frac{\partial}{\partial t}\Phi(\mathbf{r}, t) = \left(-\frac{\hbar^2\nabla^2}{2m} + V_{ext}(\mathbf{r}) + g|\Phi(\mathbf{r}, t)|^2\right)\Phi(\mathbf{r}, t)$$ (2.16)

The right hand side of Equation 2.16 can be viewed as a Hamiltonian applied to the order parameter. $|\Phi(\mathbf{r}, t)|^2$ is the local density at $\mathbf{r}$. The density term in the Hamiltonian models the fact that areas of high density tend to repel atoms because of the increased interaction rate.

Besides the local density, the order parameter also describes the local velocity. The velocity field $\mathbf{v}$ can be derived from the phase of the order parameter using the assumption that $\mathbf{v}$ is related to the local density ρ and probability current $\mathbf{J}$ by the equations

$$\mathbf{J} = \frac{\hbar}{2mi}(\Phi^\dagger \nabla \Phi - \Phi \nabla \Phi^\dagger) \tag{2.17}$$

$$\rho = |\Phi|^2 \tag{2.18}$$

$$\mathbf{v} = \mathbf{J}/\rho. \tag{2.19}$$

After splitting Φ into a real valued magnitude and a phase factor $\Phi = \rho e^{iS}$, this form can be substituted into Equations 2.17 and 2.19 to yield

$$\mathbf{v} = \frac{\hbar}{m} \nabla S. \tag{2.20}$$

This expression for the local velocity will prove useful in the discussion of vortices.

Chapter 3

The Apparatus

3.1 The BEC Machine

Our BEC apparatus is the product of the tireless work of countless physicists. The efforts in our lab that finally culminated in the first BEC seen at M.I.T. involved research that supported the preparation of many Ph.D. theses. Needless to say, this apparatus is far too complex to describe in detail here. However, I will briefly list the major stages in cooling sodium atoms from 250°C to less than 100 nK above absolute zero.

The apparatus consists of a large stainless-steel vacuum chamber connected by a long thin slowing tube to a sodium oven. In the oven liquid sodium is vaporized at 250°C . Atoms escape the oven region through a nozzle and then fly through the Zeeman slower. They enter the slower with a speed of 500 m/s and exit the other end at only 30 m/s, corresponding to a temperature of 1 K. These slow atoms are caught in a magneto-optical trap (MOT), where they are stored and further cooled to 50μK. Finally the atoms are transferred to a magnetic trap, and the hottest ones are selectively removed by RF-evaporation. This last stage reduces the temperature to 100 nK, which is far below the BEC transition temperature 740 nK for 10^7 atoms.

The final product of these three successive cooling stages is a small cloud of ultra-cold atoms magnetically suspended in a vacuum chamber. Our BEC has the shape of a cigar that is 100μm and 20μm thick, containing from 1 to 10 million atoms at a temperature of 100 nK. This tiny blob of highly degenerate matter is the starting point for all of our

scientific work, including the present study.

3.2 Cutting and Stirring

We use light forces to create both the optical knife that cuts one condensate into two separate halves and the spoon that stirs the condensate. Light forces are caused by an intensity-dependent and frequency-dependent shift of the atomic energy levels. When an atom is exposed to an electric field that oscillates at a frequency far from an atomic resonance, the lower energy level is shifted by

$$\Delta E = \frac{\hbar \Gamma^2}{8\Delta} \frac{I}{I_{sat}} \tag{3.1}$$

where I is the light intensity, Δ is the detuning from resonance, $I_{sat(Na)} = 6\text{mW/cm}^2$ is the saturation intensity, and $\Gamma_{Na} = 2\pi \times 10\text{MHz}$ is the line width.

The optical knife consists of green light focussed into a narrow sheet of $75\text{x}12\mu\text{m}$ FWHM. Its intensity corresponded to a light shift of 3 kHz, which is just strong enough to overcome the chemical potential of the condensate. Our optical spoon was just a tightly focussed spot of $12\mu\text{m}$ diameter (FWHM) of the same intensity as the knife. It was swept through the condensate by varying the frequency of a deflector AOM. The stirring process is depicted in Figure 2 of Appendix A.

Our optical utensils are made of green laser light (532 nm) from a frequency-doubled Nd:YAG laser. This light is collected in a single-mode optical fiber near the laser and then routed into the BEC lab. An intensity stabilization and control scheme has been implemented that measures the light intensity exiting the fiber using a photodiode and compares it to an external voltage representing the desired intensity. An AOM before the fiber attenuates the light to the desired intensity using a feedback circuit. This way the intensity is controlled to within 0.5% of the total intensity.

Chapter 4

Interference and Vortices

Interference between matter waves is one of the most intriguing phenomena observed in condensate physics. While interference among matter waves is a topic that is discussed theoretically in many physics classes, it is quite a different matter to find direct evidence for this effect in one's laboratory.

Previous work in our laboratory [5] showed that condensates interfere just like ordinary waves. If the order parameter (see Section 2.4) is used to simultaneously describe the condensate in two adjacent potential wells separated by a tall barrier, the phase of the two density distributions must evolve independently. When two adjacent condensates are released, the atom clouds expand, overlap, and interfere. After stirring one of the condensates with a laser beam and then imaging the density distribution of the interference pattern, we found direct evidence that the stirring motion had disturbed the condensate's phase function and created a vortices. This effort is described in detail in [14], which is attached in Appendix A.

4.1   Interference

Interference between two condensates can be understood as interference between their two order parameters. When the condensates are released from their traps, they act as two point sources of coherent atoms. To find the probability of observing an atom at any point in the interference pattern we must add the two order parameters after they have expanded

19

in space. According the GP Equation 2.16, the order parameter behaves just like a regular wave function with a density-dependent Hamiltonian. Thus, we can apply our knowledge of regular wave functions to these "macroscopic wave functions" to find the phase that the order parameter accumulates during expansion.

In ordinary wave functions the phase accumulated along a trajectory connecting one point to another is proportional to the action integral along the trajectory. We are interested in the action integral of a straight path of distance d traversed during a time interval t. The kinetic energy is then $E = \frac{1}{2}m(d/t)^2$, leading to an accumulated phase of $\int E/\hbar dt = \frac{md^2}{2\hbar t}$. Lines of constant phase difference $\Delta\phi$ between two point sources located at $\pm\frac{L}{2}\hat{\mathbf{x}}$ are then given by

$$\Delta\phi = \frac{m}{2\hbar t}(|\mathbf{r} + \frac{1}{2}L\hat{\mathbf{x}}|^2 - |\mathbf{r} - \frac{1}{2}L\hat{\mathbf{x}}|)^2 = \frac{mL\mathbf{r} \cdot \hat{\mathbf{x}}}{\hbar t}. \tag{4.1}$$

The lines of constant phase difference are thus evenly spaced straight lines with fringe separation $s = \frac{\hbar t}{mL}$, as photographed in Figure 4-1.
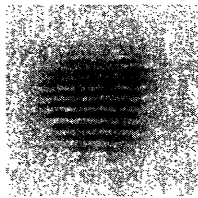

Figure 4-1: Straight interference fringes with constant spacing. Here the unit vector $\hat{\mathbf{x}}$ connecting the two source condensates points along the vertical axis. The image has a field of view of $0.4 \times 0.4\text{mm}^2$.

4.2 Vortices in BEC

Vortices are temporary BEC states of non-zero angular momentum. Their existence has long been assumed but they have eluded experimental study in gaseous BEC until a recently. After the initial observation of vortices [15, 16] progress was made in creating systems with large numbers of interacting vortices [17]. These studies all rely on density depletion at the vortex core to observe vortices. Our interference technique images the effects of vortices on the phase function of the order parameter. This allows us to see the direction of vortex rotation and thereby detect vortex-antivortex pairs.

When a laser beam is dragged through the BEC, the density is disturbed due to depletion at the beam center. This is equivalent to dragging a stick through a fluid. The velocity field of the fluid must change because the fluid flows to accommodate the stick's motion. Bose condensates behave the same way, and when the laser beam is dragged quickly enough vortices form [18]. Vortices spawned by dragging an object through a fluid always form in pairs of opposite circulation to preserve angular momentum.

4.3 Quantization of Vortices

According to Equation 2.20, the phase function is directly related to the velocity field within the condensate. Using a well-known theorem of vector calculus Equation 2.20 can be integrated along any path between two points to yield

$$\int_i^f \mathbf{v}(\mathbf{r}) \cdot d\mathbf{r} = \frac{\hbar}{m}(S_f - S_i). \tag{4.2}$$

If the initial and final points are chosen to be the same, then S_f and S_i can differ only by integer multiples of 2π. This condition means that vortices are quantized, since from a continuous range of possible values only a discrete set are allowed.

4.4 Vortices in Interference

When a condensate containing a vortex interferes with a regular condensate the phase gradient due to the vortex flow field modifies the interference pattern. This shows up as a fork in the interference fringes near the vortex. The direction of the fork is determined by the direction of circulation. Figure 4-2 shows an example of such a fork. A detailed description of this phenomenon appears in Appendix A.
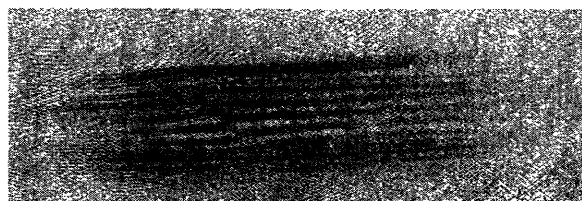

Figure 4-2: A fork in the interference fringes due to a vortex. The field of view is $1 \times 0.3\text{mm}^2$.

Chapter 5

An Improved Absorption Imaging System

In most of our BEC experiments, including the vortex study, we acquire data by recording images of the atom cloud. It is important that the image quality be as good as possible in order to extract the maximum amount of useful information. During our vortex experiments we were often confused by patterns in the image background that caused uncertainty about whether an apparent vortex was real or just an image artifact. Such background patterns have been a persistent nuisance in this apparatus, and I have developed a technique that reduces them substantially by sweeping the illuminating beam through the optical system.

5.1 Absorption Imaging

Our standard imaging technique is absorption imaging. It records the shadow cast by an atomic cloud which is allowed to expand ballistically for 20-50 ms. Expansion effectively magnifies the condensate, allowing us to observe details of the cloud that would otherwise be too small to resolve. In the vortex experiment expansion was necessary so that each interference fringe occupied at least a few camera pixels. These ballistic expansion images are, somewhat misleadingly, referred to as "time-of-flight" images (TOF).

TOF imaging recreates the optical absorption of the atomic cloud shown in Figure 5-1(d) from the three separate image frames in Figure 5-1(a-c). The first frame contains an image

I_a of the condensate illuminated by a short probe pulse of resonant laser light. In areas of high atomic density the light is attenuated by absorption. The second frame is an image I_b of the empty background illuminated by a second identical probe pulse. I_c consists of only the background light. The absorption image I_d is derived by first removing the background light I_c from I_a and I_b, and then taking the quotient, pixel by pixel, of the results:

$$I_d(x, y) = \frac{I_a(x, y) - I_c(x, y)}{I_b(x, y) - I_c(x, y)} \tag{5.1}$$

Figure 5-1 shows both the power of absorption imaging and the sensitivity to background fluctuations. The only reason that Figure 5-1(d) can be extracted at all from 5-1(a,b,c) stems from the fact that this method factors out the inhomogeneities in the probe beam. However, Figure 5-1(d) also shows significant large-scale patterns in the background that are obviously not due to atomic absorption. These patterns are due to changes in the probe beam during the few seconds between exposures (a) and (b).

We have found that the inhomogeneity of the probe beam is due to interference of the main probe beam with multiple internal reflections from the vacuum chamber windows. When examining the beam profile before the vacuum chamber it looks perfectly smooth, but after the vacuum chamber it appears very grainy, as seen magnified in Figure 5-1(a). Slight motion in the apparatus or fluctuation of the air density disturbs this interference pattern, and causes substantial variation in the pattern of the background from I_a to I_b. When two images with inconsistent backgrounds are divided, the wallpaper-like pattern in Figure 5-1(d) appears.

We have investigated the source of the probe beam fluctuations with the goal of reducing or correcting for them. One explanation is that the beam simply moves from frame to frame, and as a consequence Equation 5.1 divides the wrong pixels by one another. To test this the motion of a small spot whose beam path largely coincided with the probe beam was recorded in Figure 5-2. It appears that beams do indeed wander on the camera. However, previous efforts to correct for beam motion by shifting the relative positions of I_a and I_b before applying Equation 5.1 failed. The most plausible explanation for probe beam inconsistency is that the relative phase of the various beam paths changes between

frames. When these paths interfere they create the pattern in Figure 5-1(a) and (b), but when their phase changes the illumination pattern varies unpredictably. Different parts of the background move seemingly independently in different directions, and previously dark areas get brighter, while previously bright areas get darker. Unfortunately such changes are not amenable to corrective measures in the imaging software.
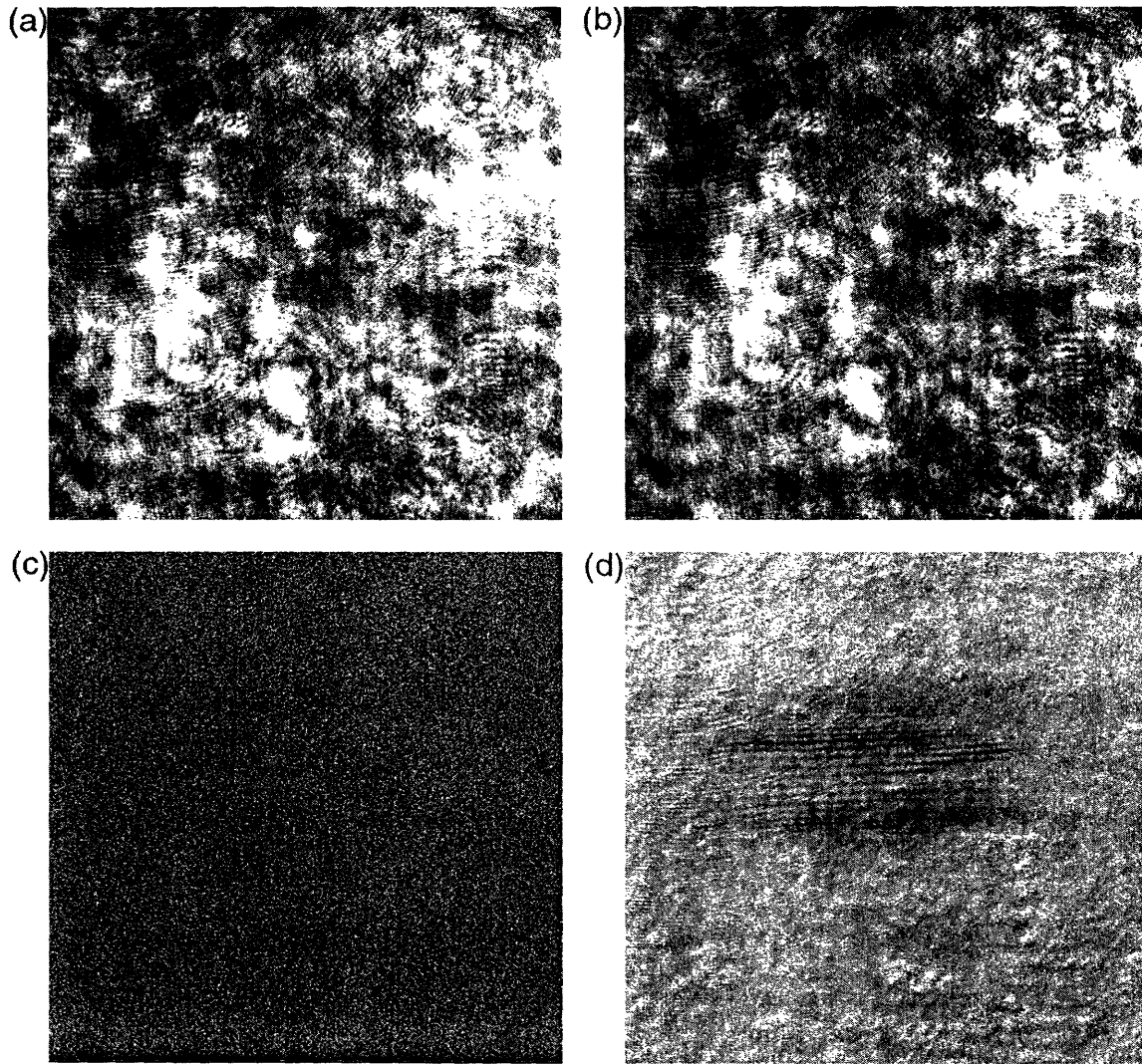

Figure 5-1: Absorption image processing. A keen eye is needed to discern the illuminated atoms in (a). An identical illuminating pulse without atoms is imaged in (b). The background light is recorded in (c), and the calculated absorption image appears in (d). Image (c) is shown in a compressed grey-scale and would be entirely black on the same scale as (a) and (b). The field of view of each frame is $1.2 \times 1.2 \text{mm}^2$.
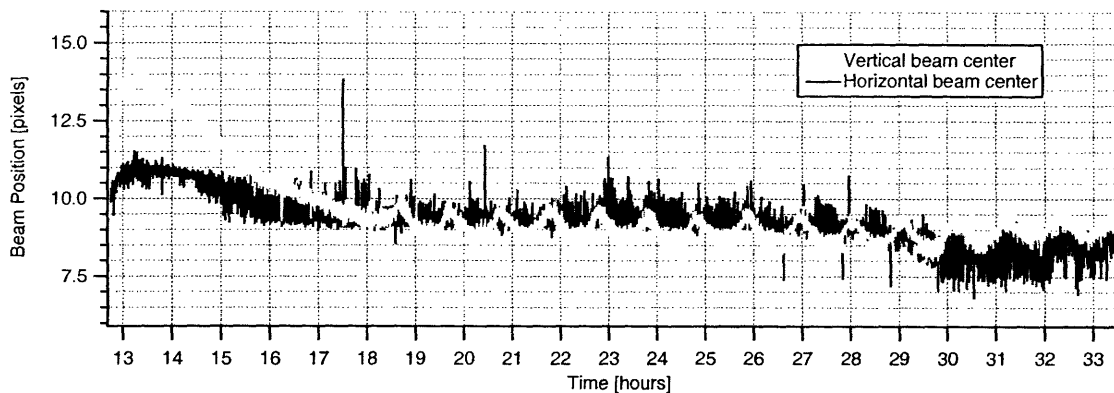
Figure 5-2: Long-term X-Y motion of a spot on the camera. The periodic motion of the vertical beam center is probably due to a ventilator turning on and off at regular intervals. Short-term jitter is less than 1 pixel when the experiment is turned off, but increases to 1-2 pixels during experiments, leading to non-statistical background noise in absorption images.

5.2   Spatial Averaging of the Probe Beam

Since the background variations are due to fluctuations in the non-uniform probe beam, sweeping the beam through a large angle averages out the sensitive portions of the interference pattern in the beam. Such a sweep is accomplished by placing two 90 MHz Accusto-Optical Modulators (AOMs) into the probe beam path as shown in Figure 5-3. The two AOMs are arranged so that their internal sound waves propagate in opposite directions. The first order diffraction peak of the first AOM passes through the second AOM whose negative first order peak is used to illuminate the atoms. In this configuration the first AOM adds its drive frequency to the light, and the second AOM subtracts the same frequency. Since the deflection of both AOMs acts in the same direction while their frequencies cancel, it is possible to sweep the beam angle without affecting the frequency. This scheme is necessary because detuning the probe beam would quickly drive it off resonance from the atomic transition used to image the atoms, making the atoms invisible.

In order to achieve a wide sweep while still illuminating the atoms a lens is placed after the AOMs which images the AOMs onto the atoms. This way any change in angle at the AOM results in the use of a different path in the optical system while still illuminating the condensate. Different beam paths are unlikely to create the same interference pattern on the camera, so sweeping the beam angle smears out most of the bothersome interference.
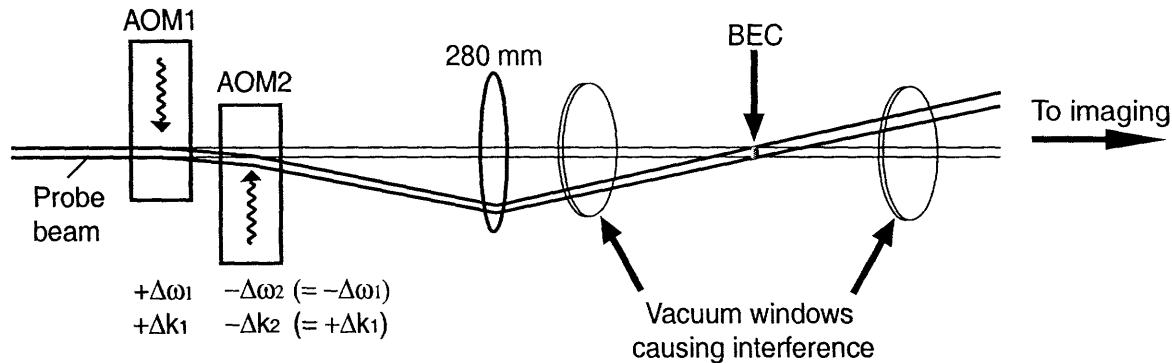
26

Figure 5-3: Optical configuration of the scanning probe beam. The probe beam passes through two AOMs whose acoustic waves have the same frequency but travel in opposite direction. By using the first order peak of AOM1 and the negative first order peak of AOM2, the frequency offsets cancel out, why the change in direction is reinforced. The AOMs are imaged onto the condensate by the 280 mm lens so that the AOM deflection can change the beam path while still illuminating the condensate.

5.3 Fast Sweep of the Probe Beam

In our interference experiment the probe beam illuminates the condensate for only $20\mu s$ in order to minimize blurring. Thus the minimum useful sweep rate of the AOM is 25 kHz[1]. If the AOM sweep is driven by a function generator that is asynchronous with the illuminating pulse, many repeated sweeps are needed to minimize inconsistencies between pulses. In this case the 100 kHz control bandwidth of the Voltage Controlled Oscillator (VCO) driving the AOMs allows for at most 4 sweeps, which would produce disastrous images when timed asynchronously. In order to sweep the AOM frequency synchronously and consistently a circuit was constructed allowing the digital control line that switches on the probe pulse to simultaneously trigger the frequency ramp.

The schematic of the frequency ramping circuit is shown in Figure 5-4. First the difference between the digital control signal and a threshold voltage is passed to an integration stage. This integrator turns the input, which is a series of digital step functions, into triangle waves which are then passed to the VCO in order to linearly ramp the frequency. The VCO output frequency is split into two parallel RF amplification stages which drive the two AOMs at precisely the same frequency. We typically sweep the AOM frequency by $B_s = 5\text{MHz}$ while the sound propagation velocity in the AOM crystals is $v_s = 4.2\text{mm}/\mu s$,

---

[1]Only one half of each wave is needed per sweep.

thereby deflecting the probe beam by $\Delta\theta = 2B_s\lambda/v_s = 1.3\text{mrad}$
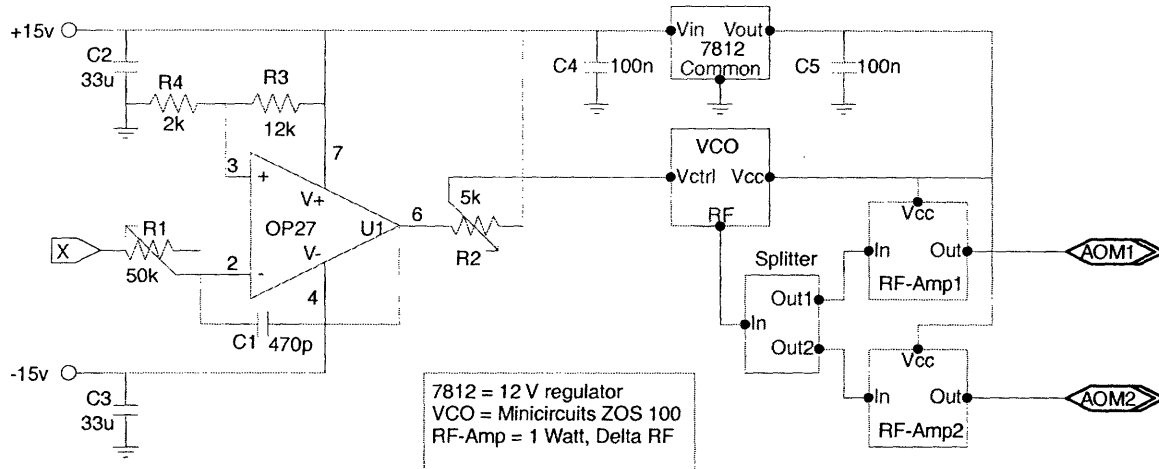

Figure 5-4: Diagram of the frequency ramping circuit. When a digital trigger pulse enters at X from the right, the RF drives for the AOMs are ramped at a constant rate set by R1. The center frequency is controlled by R2.

5.4 Quality of Scanning Probe Images

The ultimate merits of the above system depend on what effect they have on the image quality. Figure 5-5 shows four typical images with and without the scanning probe beam. It is clear that the image background is far more homogeneous with the scanning beam. Another benefit shown in Figure 5-6 is that the range of probe beam intensities is far narrower with a scanning beam. This means that the atomic saturation parameter varies less across the image, and that the likelihood of getting distracting hot spots due to zero pixel counts is reduced.
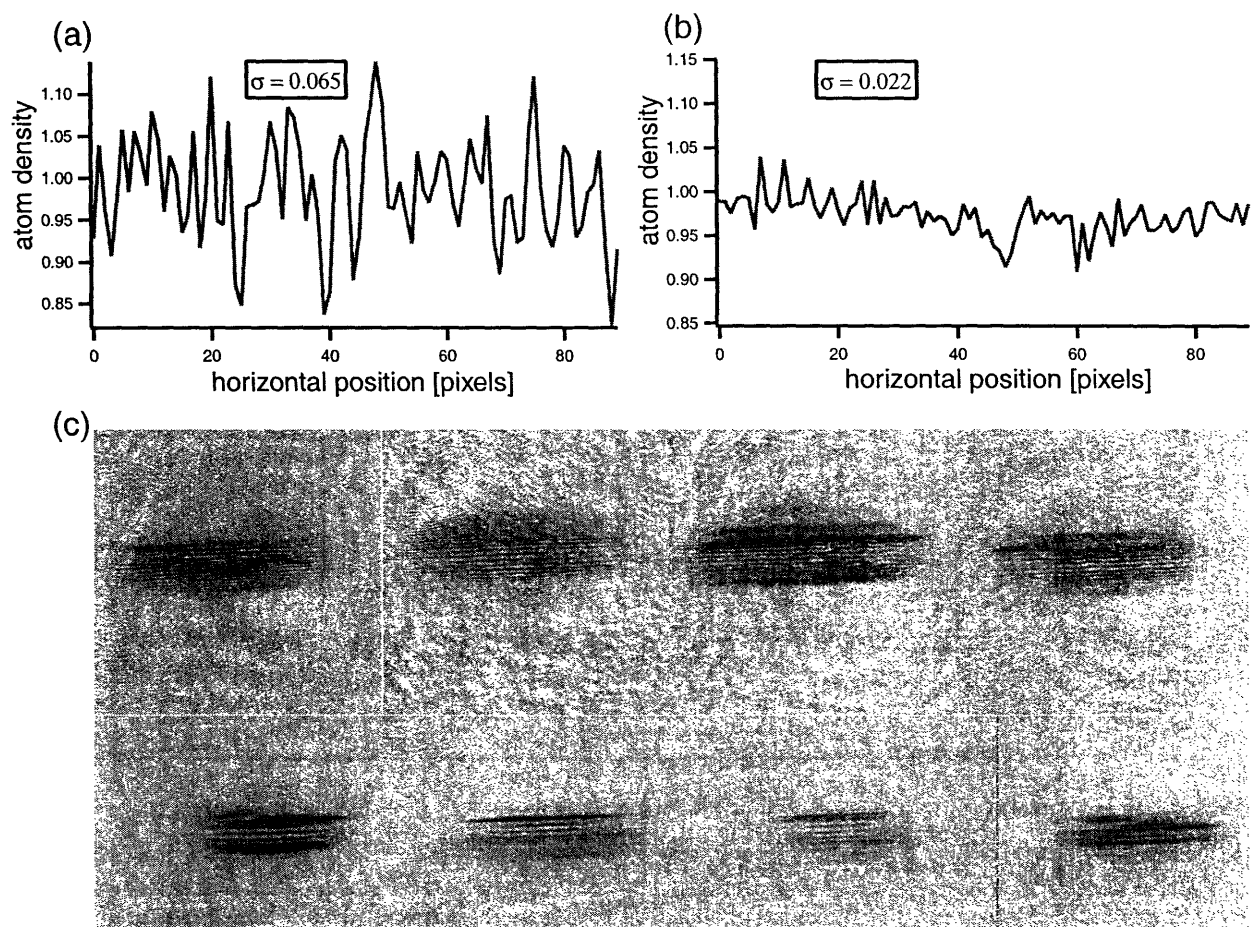
Figure 5-5: Background improvement due to AOM sweep. The first row of (c) consists of randomly chosen images from an interference run before the AOM sweep was installed. A set of images randomly chosen from a data set recorded after the sweep was installed appears in the bottom row of (c). The combined field of view of (c) is $5 \times 2\text{mm}^2$. The plot in (a) shows a horizontal trace of the background level of a typical image (after 3x3 binning) without AOM scan. Plot (b) shows the same horizontal trace with AOM scan. The standard deviation has improved by a factor of three, leading to the conclusion that the SNR of size 3x3 features is tripled by the AOM scan.
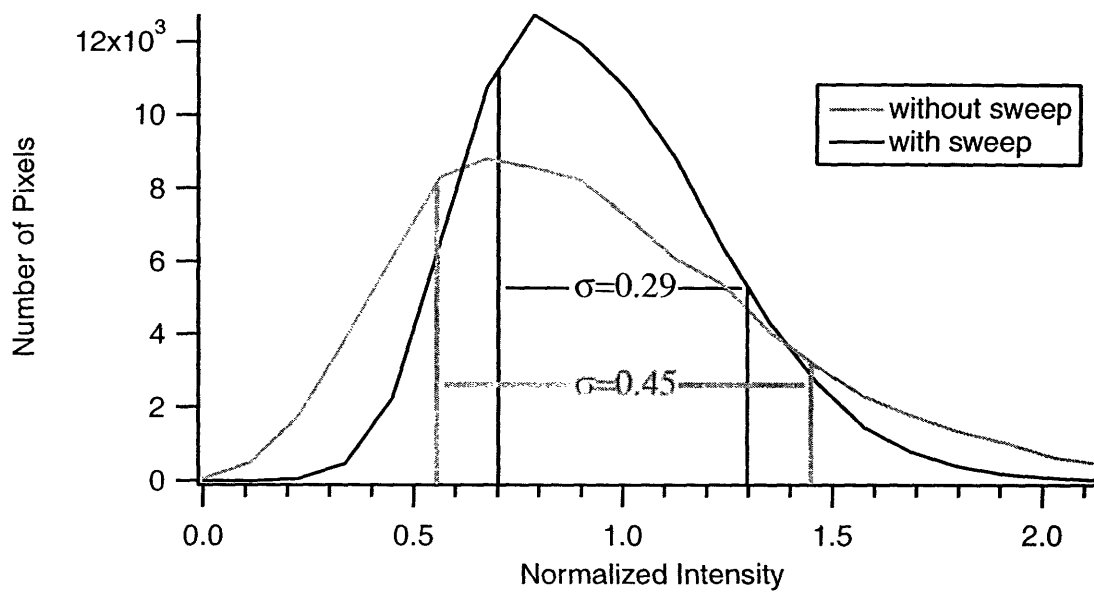
Figure 5-6: Histogram of pixel intensities. The intensities of two probe beam images were normalized, and their pixel intensities binned in a histogram. The swept probe beam has a narrower distribution and far fewer counts near zero than the stationary beam.

Appendix A

Observation of vortex phase singularities in Bose-Einstein condensates

This appendix includes the following preprint [14]: S. Inouye, S. Gupta, T. Rosenband, A.P. Chikkatur, A. Görlitz, T.L. Gustavson, A.E. Leanhardt, D.E. Pritchard, and W. Ketterle, "Observation of vortex phase singularities in Bose-Einstein condensates," *cond-mat/0104444* (2001).

Observation of vortex phase singularities in Bose-Einstein condensates

S. Inouye, S. Gupta, T. Rosenband, A.P. Chikkatur,
A. Görlitz, T.L. Gustavson, A.E. Leanhardt, D.E. Pritchard, and W. Ketterle

Department of Physics, Research Laboratory of Electronics, and MIT-Harvard Center for Ultracold Atoms,
Massachusetts Institute of Technology, Cambridge, MA 02139, USA

(April 23, 2001)

We have observed phase singularities due to vortex excitation in Bose-Einstein condensates. Vortices were created by moving a laser beam through a condensate. They were observed as dislocations in the interference fringes formed by the stirred condensate and a second unperturbed condensate. The velocity dependence for vortex excitation and the time scale for re-establishing a uniform phase across the condensate were determined.

Quantized vortices play a key role in the dynamics of superfluid flow [1]. The nucleation of vortices determines the critical velocity for the onset of dissipation at zero temperature. In liquid helium, vortices are a source of friction between the normal fluid and the superfluid. Multiple interacting vortices can form a lattice or vortex tangle, depending on their geometry and charge.

Bose-Einstein condensates of dilute atomic gases offer a unique opportunity to study quantum hydrodynamics. The low density of the gas allows direct comparison with first principle theories. A condensate is characterized by a macroscopic wavefunction $\psi(\vec{r}) = \sqrt{\rho(\vec{r})} \exp(i\phi(\vec{r}))$, which satisfies a non-linear Schrödinger equation. The density $\rho(\vec{r})$ and the velocity field $\vec{v}_s(\vec{r})$ in the hydrodynamic equations can now be replaced by the square of the wavefunction ($\rho(\vec{r}) = |\psi(\vec{r})|^2$) and the gradient of the *phase* of the wavefunction

$$\vec{v}_s(\vec{r}) = \frac{\hbar}{m}\nabla\phi(\vec{r}), \tag{1}$$

where m is the mass of the particle.

Recently, vortices in a Bose-Einstein condensate have been realized experimentally and are currently under intensive study [2–5]. In most of this work, vortices were identified by observing the density depletion at the cores. The velocity field was inferred only indirectly, with the exception of the work on circulation in a two-component condensate [2]. The flow field of a vortex can be directly observed when the phase of the macroscopic wavefunction is measured using interferometric techniques. In this work, we created one or several vortices in one condensate and imaged its phase by interfering it with a second unperturbed condensate which served as a local oscillator.

Interferometric techniques have previously been applied either to simple geometries such as trapped or freely expanding condensates [6–8], or to read out a phase imprinted by rf- or optical fields [2,9,10]. Here we apply an interferometric technique to visualize turbulent flow.
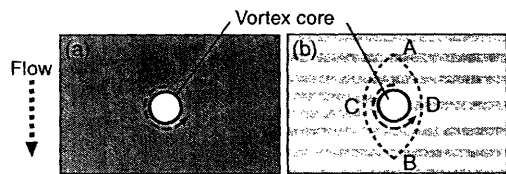

FIG. 1. Density (a) and phase (b) profile of a moving condensate with singly-charged ($n = 1$) vortex. The density profile shows the vortex core, whereas the phase pattern features a fork-like dislocation at the position of the vortex. Interference between two initially separated, freely expanding condensates produces exactly the same pattern as shown in (b), if one of the condensate contains a vortex.

The line integral of Eq. (1) around a closed path gives the quantization of circulation:

$$\int \vec{v}(\vec{r}) \cdot d\vec{r} = \frac{\hbar}{m}\left(\phi(\vec{r}_f) - \phi(\vec{r}_i)\right). \tag{2}$$

If the path is singly connected, there is no circulation. If the path is multiply connected (like around a vortex core) the circulation can take values nh/m (integer multiples of h/m), since the phase is only defined modulo 2π. As a result, the phase accumulated between two points A and B can be different depending on the path (Fig. 1). The integer quantum number n is called the charge of the vortex. When the phase gradient is integrated along a path to the left of the vortex (path ACB), the accumulated phase differs by $2n\pi$ from the path to the right (ADB).

This phase difference can be visualized with interferometric techniques. When two condensates with relative velocity v overlap, the total density shows straight interference fringes with a periodicity h/mv. If one of the condensates contains a vortex of charge n, there are n more fringes on one side of the singularity than on the other side (Fig. 1b). The change in the fringe spacing reflects the velocity field of the vortex. An observation of this fork-like dislocation in the interference fringes is a clear signature of a vortex [11].

Our setup for the interferometric observation of vortices is essentially a combination of two experiments conducted in our lab in the past [6,12]. Briefly, laser cooled sodium atoms were loaded into a double-well potential and further cooled by rf-induced evaporation below the BEC transition temperature. The double-well potential was created by adding a potential hill at the center of a cigar-shaped magnetic trap. For this, blue-detuned far off-resonant laser light (532 nm) was focused to form an elliptical $75\,\mu$m $\times$ 12 μm (FWHM) light sheet and was aligned to the center of the magnetic trap with the long axis of the sheet perpendicular to the long axis of the condensate. The condensates produced in each well were typically 20 μm in diameter and 100 μm in length. The height of the optical potential was $\sim$ 3 kHz, which was slightly larger than the chemical potential of the condensate. A more intense light sheet would have increased the distance between the condensates, thus reduced the fringe spacing [6].

After two condensates each containing $\sim 1 \times 10^6$ atoms in the $F = 1, m_F = -1$ state were formed in the double-well potential, we swept a second blue-detuned laser beam through one of the condensates using an acousto-optical deflector (Fig. 2). The focal size of the sweeping laser beam (12 μm $\times$ 12 μm, FWHM) was close to the width of the condensate. The alignment of this beam was therefore done using an expanded condensate in a weaker trap where the beam profile created a circular "hole" in the condensate density distribution.
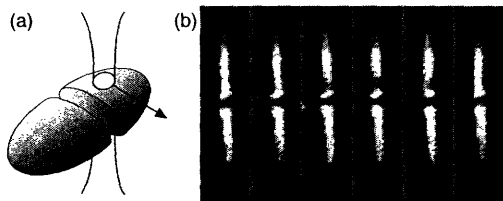

FIG. 2. Schematic (a) and phase-contrast images (b) of the condensates used for the experiment. A blue-detuned laser beam (not shown in the figure) was focused into a light sheet separating the two condensates in the magnetic trap. Another tightly focused laser beam was swept through one of the condensates (the upper one in image (b)) to excite vortices. The intensity of each laser beam was a factor of four higher than in the experiments to enhance the depleted regions in the images. The images in (b) have a field of view of 100 μm $\times$ 380 μm. For each image, the stirrer was advanced from left to right by 5 μm.

After sweeping the beam once across the "sample" condensate, the magnetic and optical fields were switched off and the two condensates expanded and overlapped during 41 ms time-of-flight. The atoms were then optically pumped into the $F = 2$ hyperfine ground state for 80 μs and subsequently probed for 20 μs by absorption imaging

tuned to the $F = 2$ to $F' = 3$ cycling transition.

Obtaining high contrast interference fringes ($\sim$ 70%) across the whole cloud required attention to several key factors. First, standard absorption imaging integrates along the line of sight, which was vertical in our experiment. Any bending or distortions of the interference fringes along the direction of observation would result in a loss of contrast. This was avoided by restricting the absorption of the probe light to a thin horizontal slice. The optical pumping beam was focused into a light sheet of adjustable thickness (typically 100 μm, which is about 10% of the diameter of the cloud after the time-of-flight) and a width of a few millimeters. This pumping beam propagated perpendicularly to the probe light and parallel to the long axis of the trap. Second, the number of atoms in the condensates had to be reduced to about 1×10^6 (corresponding to a chemical potential $\mu \sim 2.5$ kHz). Higher numbers of atoms resulted in a severe loss of contrast, even if we detuned the probe beam to reduce optical density. We suspect that at high density, the two condensates do not simply interpenetrate and interfere, but interact and collide. Third, high spatial homogeneity of the probe beam was important to obtain absorption images with low technical noise. In some of our experiments, the probe beam position was actively scanned to smooth the beam profile. Fourth, the intensity of the sweeping blue-detuned beam was adjusted so that the height of the optical potential was a fraction (typically one half) of the chemical potential of the condensate. Higher intensity of the sweeping beam resulted in reduced interference fringe contrast, probably due to other forms of excitations.

Images of interfering condensates show a qualitative difference between stirred (Fig. 3(b-d)) and unperturbed states (Fig. 3(a)). Fork-like structures in the fringes were often observed for stirred condensates, whereas unperturbed condensates always showed straight fringes. The charge of the vortices can be determined from the fork-like pattern. In Fig. 3(b), vortices were excited in the condensate on top, and the higher number of fringes on the left side indicates higher relative velocity on this side, corresponding to counterclockwise flow. Fig. 3(c) shows a vortex of opposite charge. The double fork observed in Fig. 3(d) represents the phase pattern of a vortex pair. Multiply charged vortices, which are unstable against the break-up into singly charged vortices, were not observed.
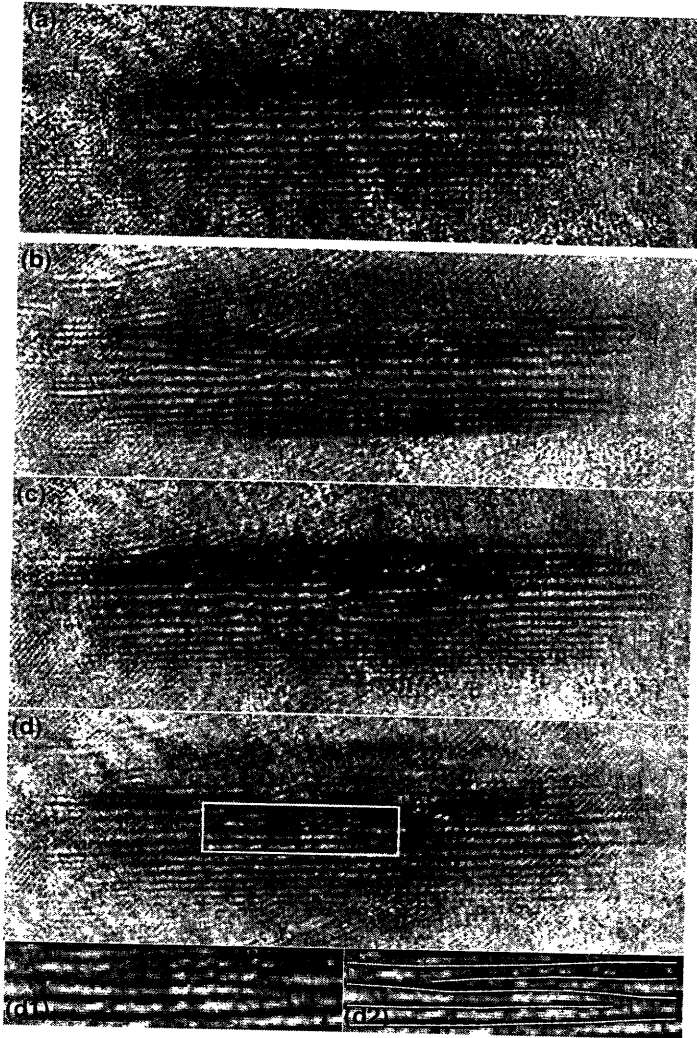
FIG. 3. Observation of the phase singularities of vortices created by sweeping a laser beam through a condensate. Without the sweep, straight fringes of $\sim 20\,\mu m$ spacings were observed (a), while after the sweep, fork-like dislocations appeared (b-d). The speed of the sweep was $1.1\,\mu m/ms$, corresponding to a Mach number of ~ 0.18. The field of view of each image is $1.1\,mm \times 0.38\,mm$. Fig. (d) shows a pair of dislocations with opposite circulation characteristic of a vortex pair. At the bottom, magnified images of the fork-like structures are shown (d1) with lines to guide the eye (d2). The orientation of the condensates is the same as in Fig. 2(b).

Theoretical studies of the superfluid flow around moving objects predict dissipationless flow below a critical velocity [1]. Above this velocity, vortices of opposite circulation are created on the two sides of the moving object and give rise to a drag force [13]. A recent experiment in our group found the onset of dissipation at a critical Mach number of $v_c/c_s \sim 0.1$ [14]. Dissipation at low velocities can not only occur by vortex shedding, but also by the creation of phonons in the low density regions of the condensate [15]. The direct observation of vortices at similar Mach numbers (Fig. 3) provides strong evidence that vortices play a major role in the onset of dissipation at the critical velocity.

By varying the speed of the laser beam sweep, we determined the velocity dependence of the vortex nucleation process. Due to the turbulent nature of the flow, every image was different even if they were taken under the same experimental conditions. Thus the images were classified by counting the number of vortices and the fractions were plotted versus the speed of the sweep (Fig. 4). The classification was done after putting images in random order to eliminate a possible "psychological bias." The plot suggests that the nucleation of vortices requires a velocity of $\sim 0.5\,\mu m/ms$, corresponding to a Mach number $v_c/c_s \sim 0.08$, consistent with our previous measurement [14]. However, a direct comparison is not possible due to different geometries—in the present experiment, the stirrer was swept along the radial direction of the condensate and almost cut the cloud completely, whereas in the previous experiment, the stirrer moved along the axial direction of an expanded condensate.
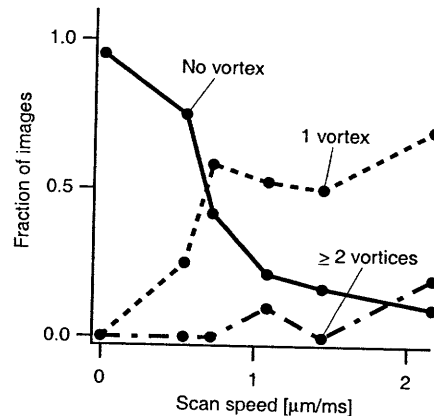

FIG. 4. Velocity dependence of vortex excitation. The fraction of images with zero (solid line), one (dashed line), and two or more vortices (dash-dotted line) are plotted versus the speed of the sweep. After the sweep, the atoms were released from the trap without delay. The total number of evaluated images was 50. Ambiguous low contrast images were excluded; therefore, the sum of the fractions is less than one.

Previous experiments have dramatically demonstrated the robustness of the long-range coherence of the condensate [6,9]. The interferometric technique used here is a sensitive way to assess whether a condensate has the assumed ground state wave function which is characterized by a uniform phase. Sweeping through the condensate excites turbulent flow. By delaying the release of the atoms from the trap by a variable amount of time, we can study the relaxation of the condensate towards its ground

state. Fig. 5 shows that the condensate completely recovers its uniform phase after $50 - 100$ ms. Vortices have disappeared after ~ 30 ms. Of course, these measurements depend crucially on the specific geometry of the cloud, but they do indicate typical time scales. The sensitivity of this method was illustrated by the following observation: in a weaker trap, we saw an oscillation in time between images with straight high contrast fringes and images with low contrast fringes. This was probably due to the excitation of a sloshing motion along the weak axis of the condensate.
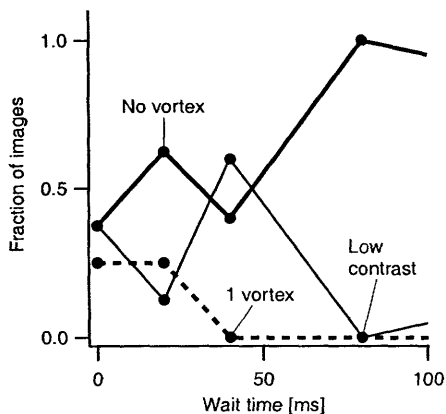

FIG. 5. Relaxation of a condensate towards uniform phase. The fraction of images with zero (thick solid line) and one (dashed line) vortex and with low contrast (thin solid line) are plotted versus the waiting time after the laser beam sweep ($v/c_s \sim 0.09$). The total number of images used for creating this plot was 33.

For interferometric detection of vortices, two different techniques have been discussed. The one employed here uses a separate condensate as a local oscillator. The other alternative is to split, shift and recombine a single condensate with vortices. In this case, the interference pattern is more complicated because all singularities and distortions appear twice. The simulations in Ref. [16] show that the self-interference technique produces more complicated fringe patterns. After completion of this work, we learned that this second technique was used in ENS, Paris to observe the phase pattern of a single vortex [17].

In conclusion, we have studied vortex excitation in Bose-Einstein condensates using an interferometric technique. This technique is suited for the study of complicated superfluid flows, e.g., when multiple vortices with opposite charges are present. We have obtained a clear visualization of vortices as topological singularities, confirmed the role of vortices in the onset of dissipation near the critical velocity, and observed the relaxation of a stirred condensate towards a state with uniform phase.
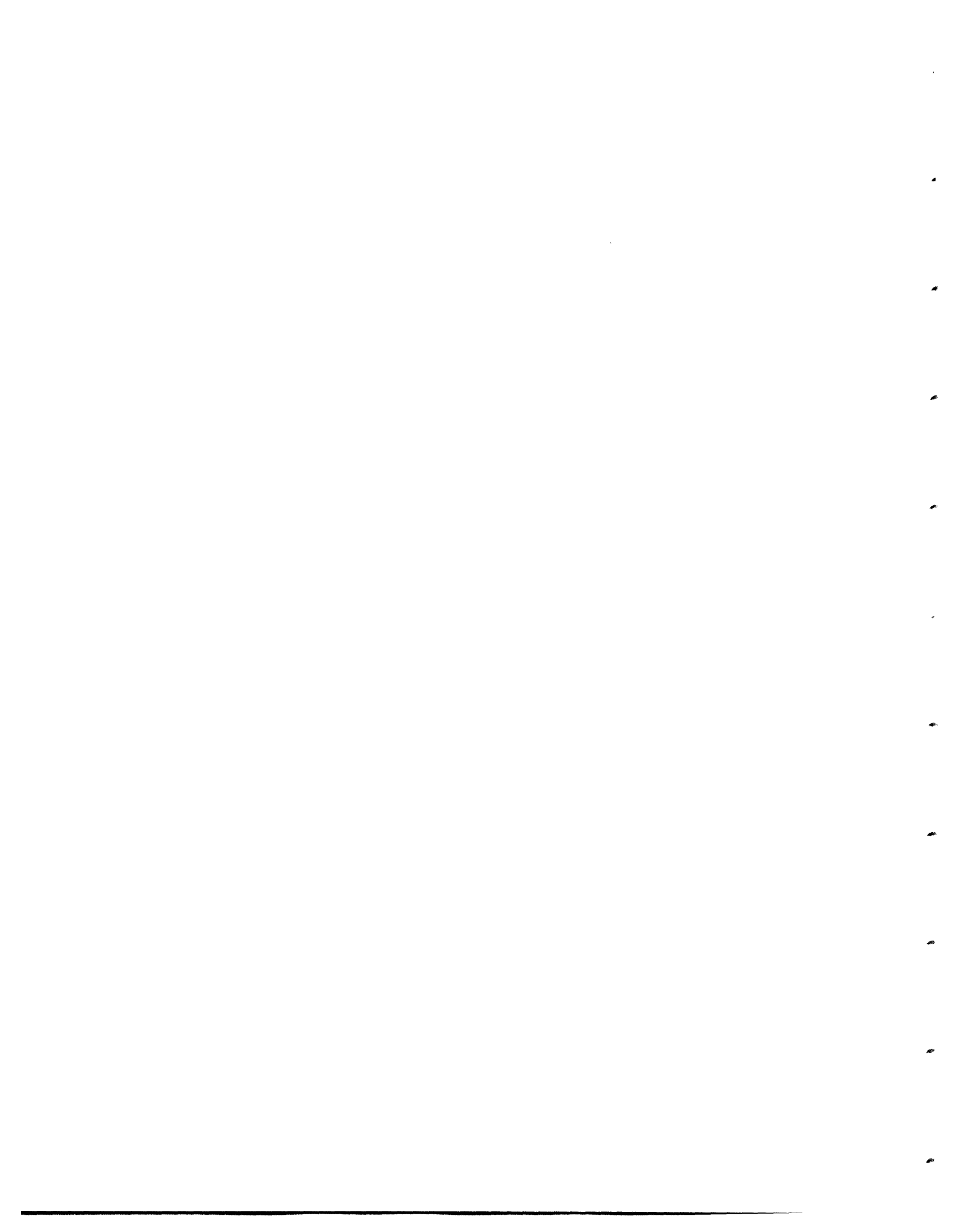
The field of Bose-Einstein condensation combines atomic and condensed matter physics. This aspect is illustrated by this work where an atomic physics technique, matter wave interferometry, was used to probe the nucleation of vortices, a problem of many-body physics. There are many issues of vortex physics which remain unexplored, including vortices in two-dimensional condensates (condensates in lower dimensions were recently realized in our laboratory [18]), pinning of vortices by additional laser beams, and interactions between vortices.

[1] R.J. Donnelly, *Quantized Vortices in Helium II* (Cambridge University Press, Cambridge, England, 1991); P. Nozieres and D. Pines, *The Theory of Quantum Liquids* (Addison-Wesley, Redwood City, CA, 1990).
[2] M.R. Matthews *et al.*, Phys. Rev. Lett. **83**, 2498 (1999).
[3] K.W. Madison, F. Chevy, W. Wohlleben, and J. Dalibard, Phys. Rev. Lett. **84**, 806 (2000).
[4] B.P. Anderson *et al.*, Phys. Rev. Lett. **86**, 2926 (2001).
[5] J.R. Abo-Shaeer, C. Raman, J.M. Vogels, and W. Ketterle, Science, in press.
[6] M.R. Andrews *et al.*, Science **275**, 637 (1997).
[7] J.E. Simsarian *et al.*, Phys. Rev. Lett. **85**, 2040 (2000).
[8] I. Bloch and T. W. Hänsch and T. Esslinger, Nature **403**, 166 (2000).
[9] D.S. Hall, M.R. Matthews, C.E. Wieman, and E.A. Cornell, Phys. Rev. Lett. **81**, 1543 (1998).
[10] J. Denschlag *et al.*, Science **287**, 97 (2000).
[11] M.R. Andrews, Ph.D. Thesis (MIT, Cambridge, MA, 1998); E.L. Bolda and D.F. Walls, Phys. Rev. Lett. **81**, 5477 (1998); J. Tempere and J.T. Devreese, Solid State Commun. **108**, 993 (1998).
[12] C. Raman *et al.*, Phys. Rev. Lett., **83** 2502 (1999).
[13] T. Frisch, Y. Pomeau, and S. Rica, Phys. Rev. Lett. **69**, 1644 (1992); T. Winiecki, J.F. McCann, and C.S. Adams, Phys. Rev. Lett. **82**, 5186 (1999). See C. Raman, R. Onofrio, J.M. Vogels, J.R. Abo-Shaeer, and W. Ketterle, J. Low Temp. Phys. **122**, 99 (2001) for further discussions.
[14] R. Onofrio *et al.*, Phys. Rev. Lett. **85**, 2228 (2000).
[15] P.O. Fedichev and G.V. Shlyapnikov, preprint cond-mat/0004039.
[16] L. Dobrek *et al.*, Phys. Rev. A, **60**, R3381 (1999).
[17] J. Dalibard, private communication.
[18] A. Görlitz *et al.*, to be published.

Bibliography

[1] Charles Kittel and Herbert Kroemer. *Thermal Physics*. W. H. Freeman and Company, New York, 2 edition, 1980.

[2] M. H. Anderson, J. R. Ensher, M. R. Matthews, C. E. Wieman, and E. A. Cornell. Observation of Bose-Einstein Condensation in a Dilute Atomic Vapor *Science*, 269:198, 1995.

[3] K. B. Davis, M.-O. Mewes, M. R. Andrews, N. J. van Druten, D. S. Durfee, D. M. Kurn, and W. Ketterle. Bose-Einstein Condensation in a Gas of Sodium Atoms *Phys. Rev. Lett.*, 75:3969–3973, 1995.

[4] C. C. Bradley, C. A. Sackett, J. J. Tollet, and R. G. Hulet. Evidence of Bose-Einstein Condensation in an Atomic Gas with Attractive Interactions *Phys. Rev. Lett.*, 75:1687, 1995.

[5] M. R. Andrews, C. G. Townsend, H.-J. Miesner, D. S. Durfee, D. M. Kurn, and W. Ketterle. Observation of interference between two Bose condensates *Science*, 275:637–641, 1997.

[6] David J. Griffiths. *Introduction to Quantum Mechanics*. Prentice Hall, New Jersey, 1995.

[7] Anthony J. Leggett. Bose-Einstein condensation in the alkali gases: Some fundamental concepts *Reviews of Modrn Physics*, 73:307–356, April 2001.

[8] F. Reif. *Fundamentals of Statistical and Thermal Physics*. McGraw-Hill, New York, 1965.

[9] W. Ketterle and N. J. van Druten. Bose-Einstein condensation of a finite number of particles trapped in one or three dimensions *Phys. Rev. A*, 54:656–660, 1996.

[10] Eric W. Weisstein. *CRC Concise Encyclopedia of Mathematics*. Chapman & Hall, New York, 1999. See entry "Partition Functions".

[11] Jeffrey Chen Gore. Electronic control of a new apparatus for studying Bose-Einstein condensation Undergraduate Thesis, Department of Physics, M.I.T., June 1999.

[12] R. K. Pathira. *Statistical Mechanics*. Pergamon, Tarrytown, New York, 1972.

[13] F. Dalfovo, S. Giorgini, L. P. Pitaevskii, and S. Stringari. Theory of Bose–Einstein condensation in trapped gases *Rev. Mod. Phys.*, 71:463, 1999.

[14] S. Inouye, S. Gupta, T. Rosenband, A.P. Chikkatur, A. Görlitz, T.L. Gustavson, A.E. Leanhardt, D.E. Pritchard, and W. Ketterle. Observation of vortex phase singularities in Bose-Einstein condensates 2001. preprint cond-mat/0104444.

[15] M. R. Matthews, B. P. Anderson, P. C. Haljan, D. S. Hall, C. E. Wieman, and E. A. Cornell. Vortices in a Bose-Einstein Condensate *Phys. Rev. Lett.*, 83:2498, 1999.

[16] K. W. Madison, F. Chevy, W. Wohlleben, , and J. Dalibard. Vortex Formation in a Stirred Bose-Einstein Condensate *Phys. Rev. Lett.*, 84:806, 2000.

[17] J.R. Abo-Shaeer, C. Raman, J.M. Vogels, and W. Ketterle. Observation of Vortex Lattices in Bose-Einstein Condensates *Science*, 292:476–479, 2001.

[18] T. Frisch, Y. Pomeau, and S. Rica. *Phys. Rev. Lett.*, 69:1644, 1992.